Verification of Filtered Two-Fluid Models for Gas-Particle Flows in Risers

Yesim Igci and Sankaran Sundaresan
Dept. of Chemical and Biological Engineering, Princeton University, Princeton, NJ 08544

DOI 10.1002/aic.12486
Published online December 29, 2010 in Wiley Online Library (wileyonlinelibrary.com).

The effect of solid boundaries on the closure relationships for filtered two-fluid models for riser flows was probed by filtering the results obtained through highly resolved kinetic theory-based two-fluid model simulations. The closures for the filtered drag coefficient and particle phase stress depended not only on particle volume fraction and the filter length but also on the distance from the wall. The wall corrections to the filtered closures are nearly independent of the filter length and particle volume fraction. Simulations of filtered model equations yielded grid length independent solutions when the grid length is ~half the filter length or smaller. Coarse statistical results obtained by solving the filtered models with different filter lengths were the same and corresponded to those from highly resolved simulations of the kinetic theory model, which was used to construct the filtered models, thus verifying the fidelity of the filtered modeling approach. © 2010 American Institute of Chemical Engineers *AIChE J,* 57: 2691–2707, 2011
Keywords: fluidization, filtered two-fluid model, sub-grid two-fluid model, coarse-grid simulations

Introduction

Gas-particle flows in bubbling and circulating fluidized beds are inherently unstable, and they manifest fluctuations in velocities and local suspension density over a wide range of length and time scales.[1,2] In riser flows, these fluctuations are associated with the random motion of the individual particles (typically characterized through the granular temperature) and with the chaotic motion of particle clusters, which play a major role in axial dispersions of particles, radial distribution of particles, chemical reaction rates, erosion, and heat transfer at the wall; in short, they affect the overall performance of circulating fluidized beds.[3–9] Although two-fluid (Euler-Euler) models[2,10,11] are able to capture these clusters in a robust manner, prohibitively expensive spatial and temporal resolutions are often needed to resolve the clusters at all length scales.[12–14] Due to computing limitations, the grid sizes used in simulating industrial scale gas-particle flows are invariably much larger than the length scales of the (finer) particle clusters. Such coarse-grid simulations for industrial scale gas-particle flows will clearly not resolve the structures which exist on sub-grid length scales; however, these small-scale unresolved structures are known to affect the resolved flow characteristics.[14–16]

Researchers have approached this problem of treating unresolved structures through various approximate schemes. O'Brien and Syamlal,[17] Boemer et al.,[18] and Heynderickx et al.[19] noted the need to correct the drag coefficient to account for the consequence of clustering and proposed corrections for the very dilute limit. Some authors have used an apparent cluster size in an effective drag coefficient closure as a tuning parameter;[20] others have deduced corrections to the drag coefficient using an Energy Minimization Multi-Scale (EMMS) approach.[21–23] Some researchers have modified the drag coefficients for homogeneous systems using a bubble-emulsion model, where the bubble and emulsion phases are described as two interpenetrating phases (to capture bed-expansion characteristics in bubbling fluidized beds with coarse grid simulations).[24,25] The concept of particle phase turbulence has also been explored to introduce the

Correspondence concerning this article should be addressed to S. Sundaresan at sundar@princeton.edu.

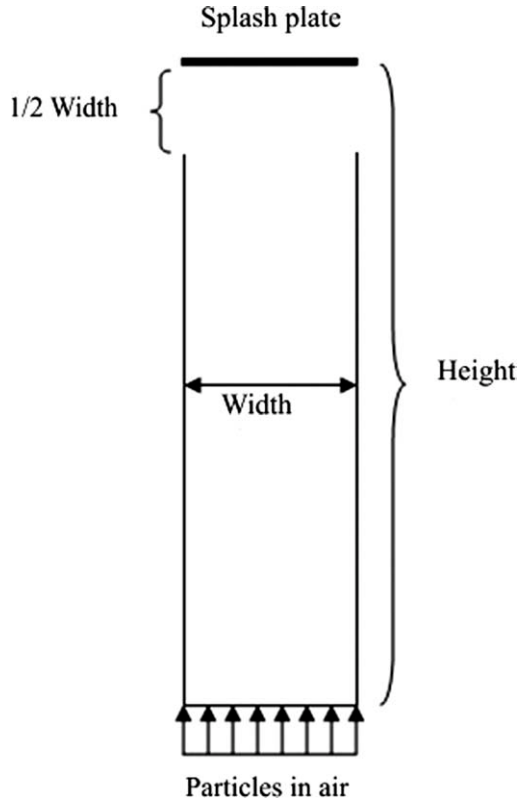

Figure 1. Schematic diagram of the 2D computational domain.

In this set-up, the gas and particles enter the domain uniformly at the bottom. A splash plate is located over the entire width at the top. The gas and particles are allowed to leave through exit regions located on either side (just below the splash plate). The height of this opening is one-half the width of the system.

effect of the fluctuations associated with clusters and streamers on the particle phase stresses.[26,27]

Agrawal et al.[12] performed highly resolved simulations of kinetic-theory-based two-fluid model (henceforth referred to as microscopic two-fluid model) equations for gas-particles flow in periodic domains, determined the domain-averaged effective drag and effective stresses, and demonstrated that these effective quantities were not only quantitatively very different from those used in the microscopic two-fluid model but also depended on size of the periodic domain. They also found that both 2D and 3D simulations revealed the same qualitative trends. Andrews et al.[28] performed highly resolved simulations of fluidized gas-particle mixtures in a 2D periodic domain whose total size coincided with that of the grid size in an anticipated large-scale riser flow simulation and constructed ad hoc sub-grid models for the effects of the fine-scale flow structures on the drag force and the stresses, and examined the consequence of these sub-grid models on the outcome of the coarse-grid simulations of gas-particle flow in a large-scale vertical riser. They found that these sub-grid scale corrections affect the predicted large-scale flow patterns profoundly.[28] In our earlier work,[29] we presented a systematic filtering approach to construct closure relationships for the drag coefficient and the effective stresses in the gas and particle phases. Briefly, we performed highly resolved simulations of a kinetic theory-based two-fluid model with Wen & Yu drag for uniformly sized particles[2,12,28–30] in a large periodic domain (considerably larger than the filter length) and filtered the results using different filter lengths. We showed that the closure relationships for the drag coefficient and the effective stresses in the gas and particle phases (that appear in the filtered two-fluid model) manifested a definite and systematic dependence on the filter length. However, these filtered closures did not include the possible effect of bounding walls and are therefore likely to be restricted to flow regions far away from solid boundaries.

An alternate approach based on the aforementioned EMMS method has been developed by Li et al.[31–35] Such an approach is reported to have good success in capturing experimental data.[22,36] Unlike this study where the corrections to the drag force depend on filter length, the EMMS model prescribes a fixed modification to the drag force and it may perhaps be viewed as the large filter length limit. Some authors[13,37–42] have combined EMMS model (which assumes that some of the particles reside in a clustered state) for drag with kinetic theory model for stresses (which assumes that individual particles move chaotically); in contrast, the approach pursued in our studies mentioned above and in this study filters the stresses and the drag in a consistent manner.

It is now generally accepted that clusters and streamers are formed in gas-particle flows in vertical risers, and they are found more frequently near the tube walls so that on an average, particle volume fraction is larger near the wall region. A consequence of such segregation is that the average velocity of particles and gas in the wall region can be downward even though the net flow is in the upward direction—a dilute rising core and a dense descending annular region.[5,6,9,15,43,44] Clusters at the wall of a riser have been observed to form, descend, break-up, travel laterally from the annulus to the core, and then be re-entrained in the upward flowing core. In this manner, they contribute to the internal solids mixing process within a riser.[7,8] Consequently, it is important to incorporate the effects of bounding walls on the filtered closures before attempting a comparison of the filtered model predictions with experimental data.

The first objective of this study is to investigate of the effect of the bounding walls on the closure relationships for the filtered two-fluid model equations and to incorporate these effects as wall corrections to the filtered drag

Table 1. Sample Physical Properties of the Gas and Particles

d_p	Particle diameter	7.5×10^{-6} m
ρ_s	Particle density	1500 kg/m^3
ρ_g	Gas density	1.3 kg/m^3
μ_g	Gas viscosity	1.8×10^{-5} kg/m s
e_p	Coefficient of restitution	0.9
e_w	e for particle-wall collisions	0.9
g	Gravitational acceleration	9.80665 m/s^2
v_t	Terminal settling velocity	0.2184 m/s
$\frac{v_t^2}{g}$	Characteristic length	0.00487 m
$\frac{v_t}{g}$	Characteristic time	0.0223 s
$\rho_s v_t^2$	Characteristic stress	71.55 kg/m s^2
$\rho_s v_t$	Characteristic mass flux	327.6 kg/m^2 s

Figure 2. Snapshots of the particle phase volume fraction field extracted from the 2D simulation of the kinetic theory model equations in a 2D domain with partial slip (Johnson and Jackson[45]) BC with (a) $\varphi = 0.0001$ and (b) $\varphi = 0.6$ for the particle phase and free slip BC for the gas phase at all walls.

Simulation conditions: The dimensionless inlet gas and particle phase superficial velocities are 4.259 and 0.109, respectively. The physical conditions corresponding to this simulation are listed in Table 1. The inlet particle phase volume fraction is 0.07. Channel width and height are 102.8 and 1028 *du*, respectively. The gray scale axis ranges from $\phi_s = 0.00$ (white) to $\phi_s = 0.45$ (black).

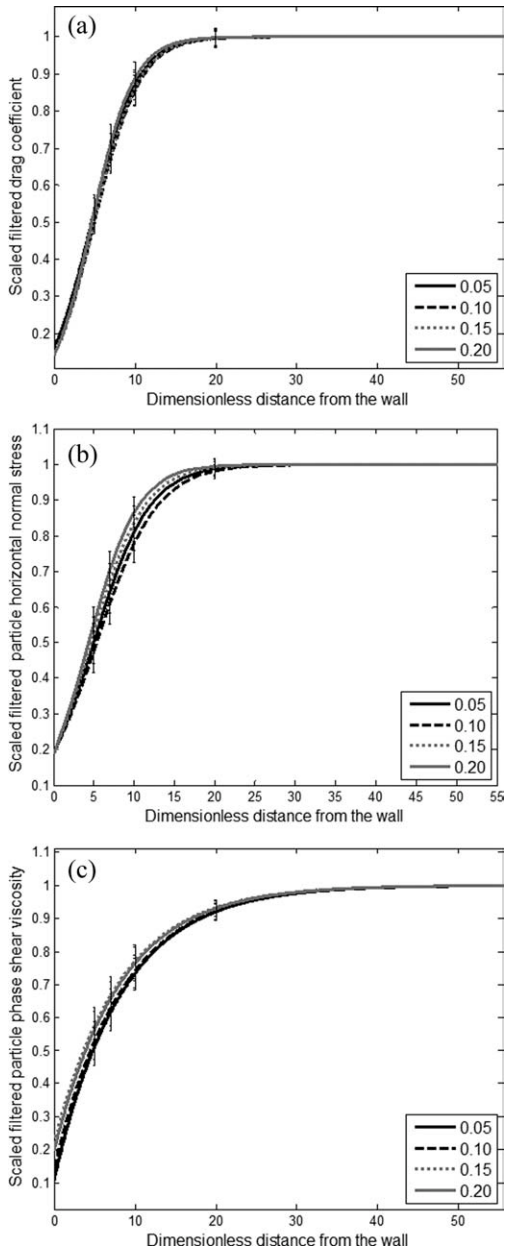

Figure 3. (a) The filtered drag coefficient, (b) the filtered horizontal particle phase normal stress, and (c) the filtered particle phase viscosity extracted from kinetic theory model-based simulations in a channel shown in Figure 1.

Error bars at four locations are also included. Results are shown for four different particle phase volume fractions inside the filtered region, illustrating that the wall correction is essentially independent of particle volume fraction. Grid length: 0.514 *du*. Filter length: 2.056 *du*. The filtered drag coefficient is scaled with that extracted from the core region. The results are shown for one-half of the channel width and the distance is measured from the wall. Channel width and height are 102.80 and 1028 *du*, respectively. The dimensionless inlet gas and particle phase superficial velocities are 4.259 and 0.109, respectively. The inlet particle phase volume fraction is 0.07. $\varphi = 0.6$. The remaining physical conditions corresponding to this simulation are listed in Table 1.

coefficient and particle phase stresses that are appropriate for coarse-grid simulations of gas-particle flows in risers (of circulating fluidized beds). To address this point, we have performed a set of highly resolved simulations of a kinetic-theory-based two-fluid model in 2D channels equipped with bounding walls and inlet and outlet regions, and analyzed the variation of the filtered closures with distance from the

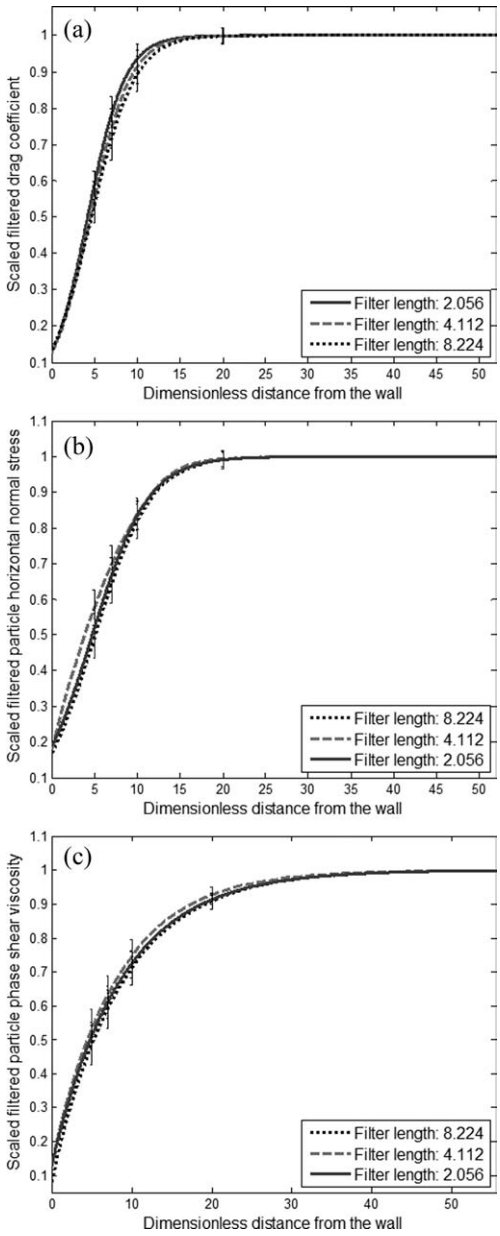

Figure 4. (a) Filtered drag coefficient, (b) filtered horizontal particle phase normal stress, and (c) filtered particle phase viscosity as functions of distance from the wall, extracted from kinetic theory model-based simulations in the channel shown in Figure 1 for three filter lengths.

Error bars at four locations are also included. Grid length: 0.514 *du*. The filtered drag coefficient is scaled with that extracted from the core region. The results are shown for one-half of the channel width and the distance is measured from the wall. See caption for Figure 3 for additional details.

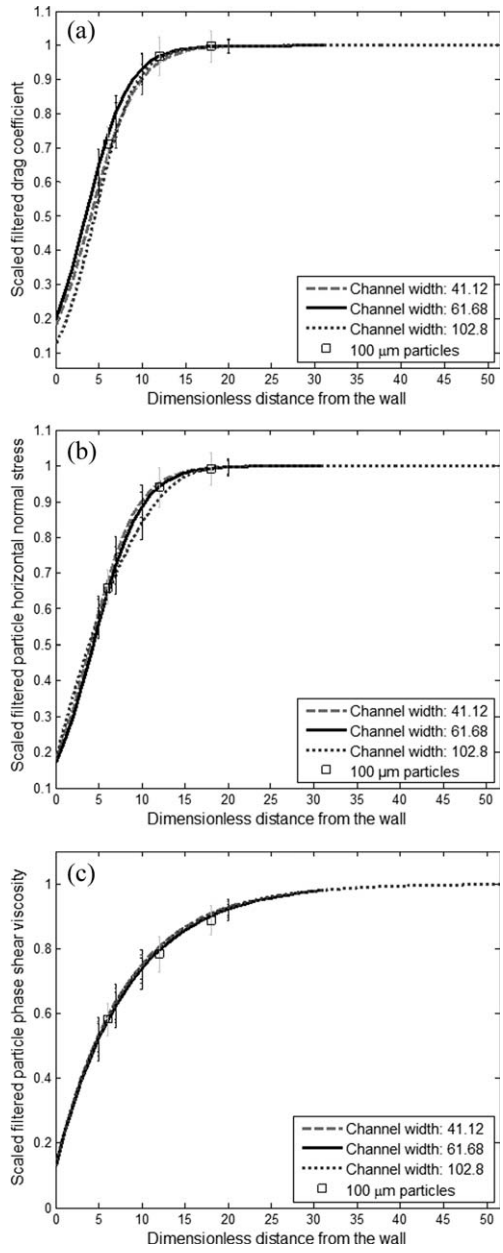

Figure 5. (a) Filtered drag coefficient, (b) filtered horizontal particle phase normal stress, and (c) filtered particle phase viscosity as functions of distance from the wall, extracted from kinetic theory model-based simulations in the channel shown in Figure 1 for three different channel widths.

Error bars at four locations are also included. Filter length: 2.056 *du*. Grid length: 0.514 *du*. All filtered quantities were scaled with the corresponding quantities extracted from the core region (which were found to be the same for all three channel widths). See caption for Figure 3 for additional details. The figure also includes three data points (with error bars) from simulations with 100 μm diameter particles.

bounding walls using different filter lengths. The present analysis reveals that the filtered quantities must be allowed to depend not only on particle volume fraction but also on the distance from the wall.

The second objective of this study is to demonstrate the fidelity of the filtered two-fluid models. This entails several tests: (a) the filtered two-fluid models must yield grid-length independent coarse statistical quantities once the grid length

Table 2. Wall Corrections to the Filtered Drag Coefficient, Horizontal Particle Phase Normal Stress, and Shear Viscosity

Dimensionless distance from the wall (see Figure 1): $x_d = g\ x/v_t^2$

1. Filtered drag coefficient:

$$\overline{\beta_{\text{filtered,scaled}}} = \frac{\overline{\beta_{\text{filtered}}}(\overline{\phi_s}, x_d)}{\overline{\beta_{\text{filtered,core}}}(\overline{\phi_s})} = \frac{1}{1 + 6.00\exp(-a x_d)}, x_d \leq \frac{\text{channel width}}{2}$$

$$\overline{\beta_{\text{filtered,core}}}(\overline{\phi_s}) = \overline{\beta_{\text{filtered,periodic}}}(\overline{\phi_s})$$

where "a" is a function of the wall specularity coefficient (φ) and is defined as:

$$a(\varphi) = 0.036\varphi^2 + 0.162\varphi + 0.295$$

2. Filtered particle phase horizontal normal stress:

For $\varphi = 0.0$ (*free slip*):

$$\overline{p_{s,\text{filtered},xx,\text{scaled}}} = \frac{\overline{p_{s,\text{filtered},xx}}(\overline{\phi_s}, x_d)}{\overline{p_{s,\text{filtered},xx,\text{core}}}(\overline{\phi_s})} = \frac{1}{1 + 9.14\exp(-0.345 x_d)}, x_d \leq \frac{\text{channel width}}{2}$$

For $\varphi = 0.6$:

$$\overline{p_{s,\text{filtered},xx,\text{scaled}}} = \frac{\overline{p_{s,\text{filtered},xx}}(\overline{\phi_s}, x_d)}{\overline{p_{s,\text{filtered},xx,\text{core}}}(\overline{\phi_s})} = \begin{cases} -0.00267x_d^2 + 0.0926x_d + 0.180, x_d \leq 14.5 \\ (1 + 25.4)(1 - \exp(-0.450x_d)) - 25.4, 14.5 < x_d \leq \frac{\text{channel width}}{2} \end{cases}$$

$$\overline{p_{s,\text{filtered},xx,\text{scaled}}}(\overline{\phi_s}) = \overline{p_{s,\text{filtered},xx,\text{periodic}}}$$

For $0 < \varphi < 1$, we can capture the effect of φ on the wall corrections with the correlation given below:

$$\overline{p_{s,\text{filtered,scaled}}} = \begin{cases} \overline{p_{s,\text{filtered,scaled},\varphi=0.0}}, \varphi = 0.0 \\ \frac{\overline{p_{s,\text{filtered,scaled},\varphi=0.6}} + (c-1)\overline{p_{s,\text{filtered,scaled},\varphi=0}}}{c}, 0 < \varphi \leq 0.6 \\ \overline{p_{s,\text{filtered,scaled},\varphi=0.6}}, \varphi > 0.6 \end{cases}$$

Here, "c" is defined as $0.6/\varphi$. For instance, $c = 2$ for $\varphi = 0.3$.

3. Filtered particle phase shear viscosity:

For $\varphi = 0.0$ (*free slip*):

$$\overline{\mu_{s,\text{filtered,scaled}}} = \frac{\overline{\mu_{s,\text{filtered}}}(\overline{\phi_s}, x_d)}{\overline{\mu_{s,\text{filtered,core}}}(\overline{\phi_s})} = \frac{1}{1 + 5.69\exp(-0.228 x_d)}, x_d \leq \frac{\text{channel width}}{2}$$

For $\varphi = 0.6$:

$$\overline{\mu_{s,\text{filtered,scaled}}} = \frac{\overline{\mu_{s,\text{filtered}}}(\overline{\phi_s}, x_d)}{\overline{\mu_{s,\text{filtered,core}}}(\overline{\phi_s})} = (1 - 0.130)(1 - \exp(-0.123 x_d)) + 0.130, x_d \leq \frac{\text{channel width}}{2}$$

$$\overline{\mu_{s,\text{filtered,scaled}}}(\overline{\phi_s}) = 1.15\overline{\mu_{s,\text{filtered,periodic}}}(\overline{\phi_s})$$

(*Continued*)

Table 2. (Continued)

For $0 < \varphi < 1$, we can capture the effect of φ on the wall corrections with the correlation given below:

$$\overline{\mu_{s,\text{filtered,scaled}}} = \begin{cases} \overline{\mu_{s,\text{filtered,scaled},\varphi=0.0}}, & \varphi = 0.0 \\ \dfrac{\overline{\mu_{s,\text{filtered,scaled},\varphi=0.6}} + (c-1)\overline{\mu_{s,\text{filtered,scaled},\varphi=0}}}{c}, & 0 < \varphi \le 0.6 \\ \overline{\mu_{s,\text{filtered,scaled},\varphi=0.6}}, & \varphi > 0.6 \end{cases}$$

Here, "c" is defined as $0.6/\varphi$. For instance, $c = 2$ for $\varphi = 0.3$.

has become sufficiently smaller than the filter length; (b) these coarse statistical quantities obtained with different filter lengths should be the same, at least for a range of filter lengths; and (c) the coarse statistical quantities obtained by solving the filtered model must match those obtained by through highly resolved solution of the microscopic two-fluid model (which was used to generate the filtered two-fluid model). It will be demonstrated in this study that all of these requirements are indeed met satisfactorily, thus establishing the viability of this approach. Finally, we will also present some results on the CPU requirements for computations using the filtered model and contrast it with those for highly resolved simulations of the microscopic two-fluid model.

The effect of bounding walls on closures for filtered two-fluid model equations

To probe the effect of solid boundaries on the closure relations, we simulated the flow of a mixture of uniformly sized particles and gas through vertical 2D channels equipped with bounding walls and inlet and outlet regions (see Figure 1). The kinetic theory-based two-fluid model equations and the associated constitutive relations used in these simulations can be found in Agrawal et al.[12] Partial slip boundary conditions (BCs) developed by Johnson and Jackson[45] were used for the tangential velocities and granular temperature (θ_s) of the uniformly sized particle phase at all walls. These BCs are as follows:

$$\mathbf{n}\cdot\underline{\underline{\sigma_s}}\cdot\mathbf{t} + \frac{\pi}{2\sqrt{3}\phi_{s,\max}}\varphi\rho_s g_o \phi_s \sqrt{\Theta_s}\mathbf{v}_{\text{sl}} = 0, \quad \mathbf{v}_{\text{sl}} = \mathbf{v} - \mathbf{v}_{\text{W}} \tag{1}$$

$$\mathbf{n}\cdot\mathbf{q} = \frac{\sqrt{3}\pi}{6\phi_{s,\max}}\varphi\rho_s\phi_s g_o \Theta_s^{1/2}|\mathbf{v}_{\text{sl}}|^2 - \frac{\sqrt{3}\pi}{4\phi_{s,\max}}(1-e_w^2)\rho_s\phi_s g_o \Theta_s^{3/2}, \quad \mathbf{q} = -\lambda_s\nabla\Theta_s \tag{2}$$

Here, φ represents the specularity coefficient, which is a measure of the fraction of collisions transferring tangential momentum to the wall and varies between zero (for smooth walls) and unity (for rough walls).[46,47] (Values ranging between 0.0001 and 0.6 have been reported to capture the macroscopic flow patterns in the literature.[48–51]) In this study, we have performed simulations for a number of different specularity coefficients between zero and one. For the gas phase, free slip BC was used at all walls. (It has already been shown that the gas/particle flow patterns in a riser are only weakly dependent on the gas phase BCs.[48]) All the simulations were done using the open-domain software MFIX.[11]

Although all the results will be presented as dimensionless variables, with ρ_s, v_t, and g as the characteristic density, velocity, and acceleration, it is instructive to consider a typical set of dimensional quantities to help visualize a representative physical system better. (See Table 1 and the notation for the nondimensionalization.) Most of the 2D filtered results with wall corrections presented in this manuscript are based on computational data gathered in a 2D channel with width and height of 102.8 and 1028 dimensionless units, respectively. This domain size corresponds to 0.5 m $\times$ 5.0 m for the 7.5×10^{-5} m FCC particles and ambient air (whose properties are given in Table 1). (Henceforth "dimensionless units" will be referred to as "*du*".) In our simulations, the gas and particles enter the channel uniformly at the bottom. The dimensionless (dimensional) inlet gas and particle phase superficial velocities are 4.259 (0.93 m/s) and 0.109 (0.0238 m/s), respectively. The inlet particle phase volume fraction is 0.07. A splash plate is located over the entire width at the top. The gas and particles are allowed to leave through exit regions located on either side (just below the splash plate). The height of this opening is one-half the width of the system. This geometry is similar to the one employed in Andrews et al.,[28] although the dimensions of the channel are now smaller to make highly resolved simulations affordable.

In each simulation, after an initial transient period that depended on the initial conditions, persistent, time-dependent, and spatially inhomogeneous structures developed (henceforth referred to as statistical steady state, SSS). Figures 2a, b show instantaneous snapshots of the particle phase volume fraction field in the SSS for simulations with wall specularity coefficients of 0.0001 and 0.6, respectively. By analyzing thousands of such snapshots, the closure relations for the filtered models were obtained with various filter lengths. The procedure to extract the filtered closure relations is similar to that used in our earlier study of flows in periodic domains but also has an important difference. When simulations are done in a periodic domain, all the cells are statistically equivalent, and therefore no distinction needs to be made about the location; the same is not true in a channel flow simulation. Therefore, the filtered results extracted by postprocessing a channel flow simulation were classified in terms of the distance from the boundaries as well as in terms of the average particle phase volume fraction inside the filtering region. It is important to note that the statistical results presented here represent averages of at least 1000 samples at each location considered in this study. Also note that the range of filtered particle volume fraction values for which one can get such a large number of samples depend on the time-averaged particle volume fraction at that

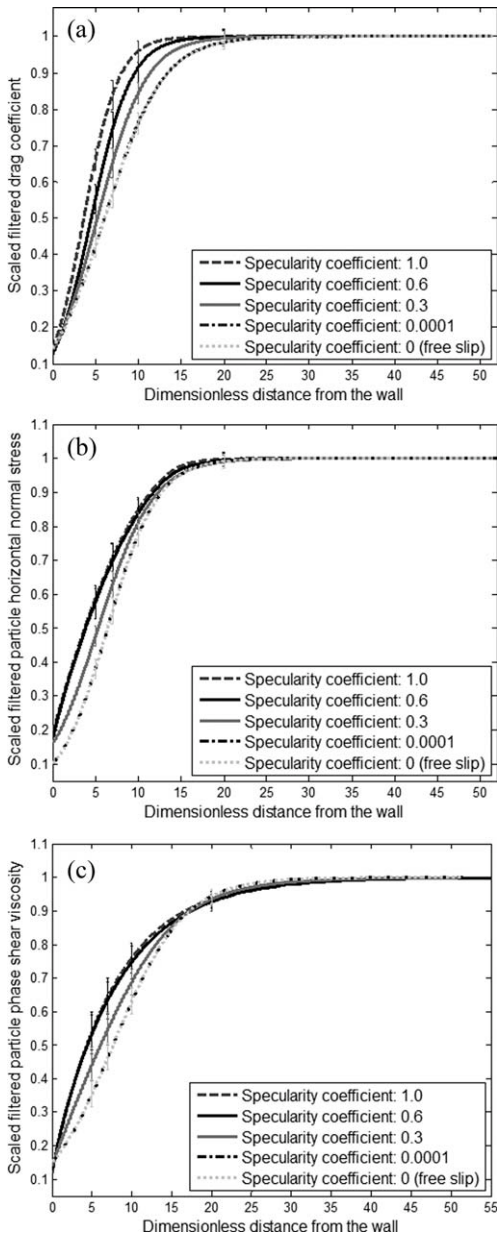

Figure 6. (a) Filtered drag coefficient, (b) filtered horizontal particle phase normal stress, and (c) filtered particle phase viscosity as functions of distance from the wall, extracted from kinetic theory model-based simulations in the channel shown in Figure 1 for specularity coefficients of 0, 0.0001, 0.3, 0.6, and 1.

Error bars at four locations are also included. Filter length: 4.112 *du*. Grid length: 0.514 *du*. Channel height: 1028 *du*. All filtered quantities were scaled with the corresponding quantities extracted from the core region. See caption for Figure 3 for additional details.

location. Further discussion of the procedure to extract filtered closure relations can be found in our earlier study,[29] Agrawal et al.[12] and Andrews et al.[28]

In this study, these kinetic-theory-based two-fluid model simulations were performed with a grid length of 0.514 *du* as anything finer was beyond our resources. Therefore, we used the data obtained at this resolution to do the filtering and all the filtered closure relations presented here are based on this grid resolution; there are minor quantitative, but not qualitative, differences between the closures obtained with 0.514 *du* grids and that presented in our earlier manuscript[29] for 0.257 *du*, but this difference is insignificant when the filter length is considerably larger than the grid length.

Figures 3a–c show the effect of the bounding walls on the filtered drag coefficient, particle phase horizontal normal stress and the particle phase shear viscosity, respectively, for four different particle volume fractions inside the filtering region and a filter length of 2.056 *du*. (We examine the horizontal normal stress as it is the most relevant normal stress component for the development of lateral segregation of particles in riser flows. The horizontal normal stress includes both the kinetic theory contribution and that arising from the mesoscale fluctuations.) All the quantities in these figures have been scaled with the corresponding values extracted from the core region (plateau values) of the channel. The filtered drag coefficient and horizontal normal stress extracted in the core were found to be very nearly the same as those obtained in periodic domain simulations at the same grid resolution, while the shear viscosity in the core was about 15% higher than that estimated in periodic domain simulations. These confirm that periodic domain simulations capture to a good accuracy the mesoscale structures in the core. In these figures, the results are shown for one-half of the channel width, and the distance is measured from the wall. It is readily seen that all three filtered quantities are significantly different in the core and the wall regions; for example, the filtered drag coefficient from the core region of the suspension is about ~five times larger than the filtered drag coefficient at the wall. The error bars showing the uncertainty in wall corrections are larger than the difference between the curves corresponding to four different particle concentrations (inside filtering regions); therefore, we can conclude that the pattern seen in this figure is essentially independent of the mean particle phase volume fraction in a filtering region. It can also be inferred that conditions outside the filtering region do not affect the statistical averages of consequences resulting from the mesoscale structures inside the filtering region; as a result, simple algebraic closure models for the drag coefficient, particle phase horizontal normal stress and shear viscosity suffice.

The dependence of the filtered closures on the distance from the walls may be rationalized as follows: it is entirely reasonable that fluctuations will be dampened in the vicinity of solid boundaries, and as a result the filtered horizontal normal stress should be diminished near the boundaries (just as in single phase turbulent flows[52]). (As the fluctuations associated with the mesoscale structures contribute to breakup of clusters, diminished fluctuations near the boundaries result in larger clusters and hence lower drag coefficient. The wall effect seen in the filtered horizontal normal stress and drag coefficient appear to extend to approximately the same distance away from the wall, while that for the shear viscosity effect is seen to persist for a little further away from the wall.

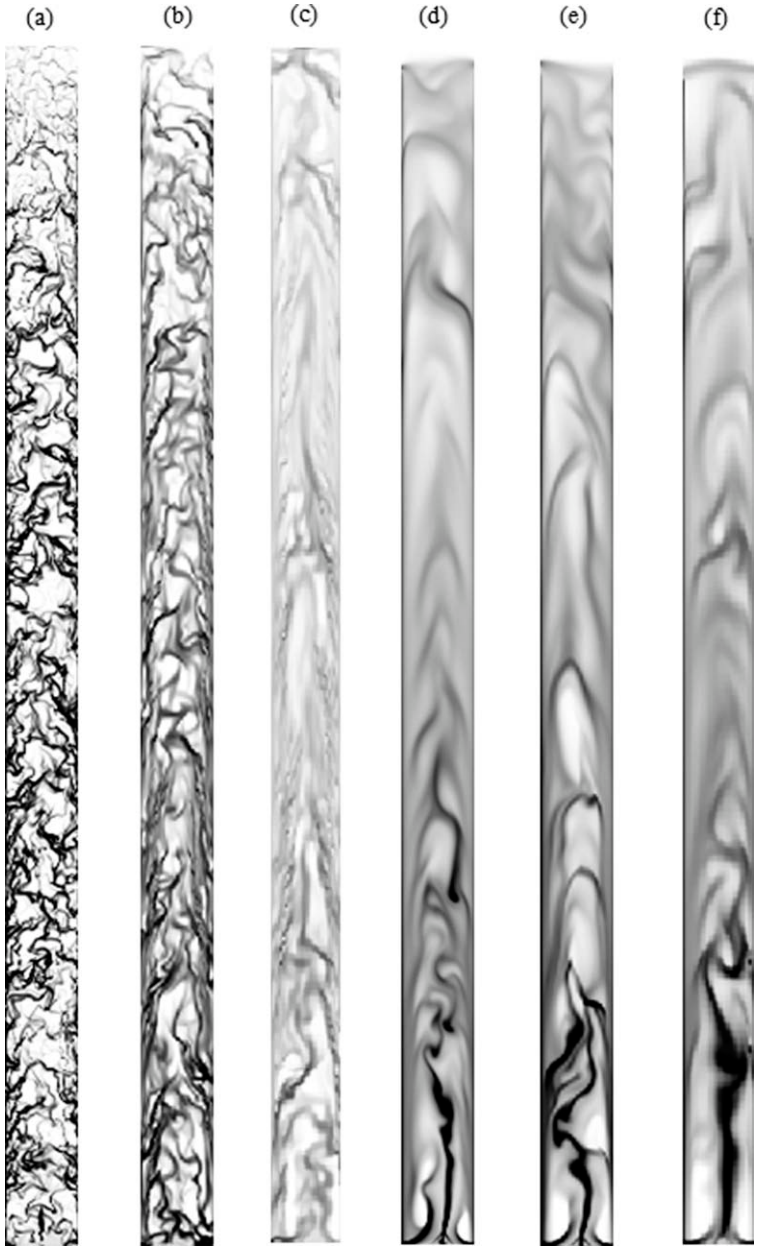

Figure 7. Snapshots of the particle phase volume fraction field extracted from the 2D simulation of (a) the kinetic theory model equations with 0.514 *du* grids, (b) the kinetic theory model equations with 1.028 *du* grids, (c) the kinetic theory model equations with 2.056 *du* grids, (d) the filtered model equation with 0.514 *du* grids, (e) the filtered model equation with 1.028 *du* grids, (f) the filtered model equation with 2.056 *du* grids.

Wall corrections (extracted from kinetic theory simulations with $\varphi = 0.6$) were included in the closures for the filtered model equations. Simulation conditions: The dimensionless inlet gas and particle phase superficial velocities are 4.259 and 0.109, respectively. The physical conditions corresponding to this simulation are listed in Table 1. The inlet particle phase volume fraction is 0.07. Free slip BC was imposed for both phases at all walls for simulations of the filtered models, whereas in the kinetic theory-based simulations, partial slip BC for the particle phase ($\varphi = 0.6$) and free slip BC for the gas phase were used. Channel width and height are 61.68 and 1028 *du*, respectively. The gray scale axis ranges from $\phi_s = 0.00$ (white) to $\phi_s = 0.45$ (black).

Having ascertained that the wall corrections to the filtered closures are nearly independent of the mean particle volume fraction in the filtering region, we performed the rest of the analysis by aggregating the results obtained at various filtered particle phase volume fractions. The effect of the filter length on the wall corrections to the filtered drag coefficient, filtered particle phase horizontal normal stress, and shear viscosity are shown in Figures 4a–c, respectively, for three filter lengths (2.056, 4.112, and 8.224 *du*). All three quantities have been scaled by the respective values in the core region, which depends systematically on filter length; however, the scaled quantities presented in these figures are nearly independent of filter length (to within the error bars shown). In other words, the filter length dependence of the filtered closures is essentially independent of the distance from the wall.

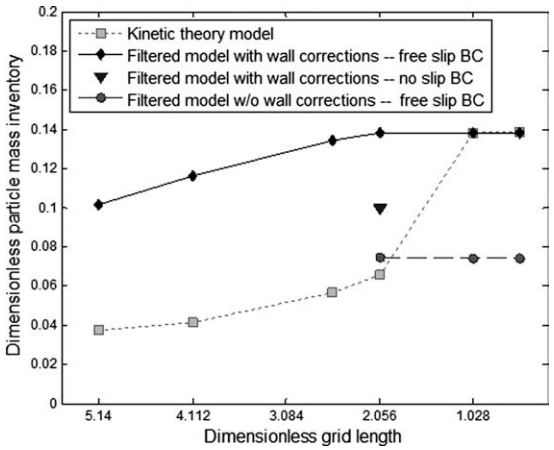

Figure 8. The variation of the particle mass inventory with grid resolution in the channel, determined from simulations of the kinetic theory-based model and the filtered model (corresponding to a filter length of 4.112 *du*) with and without wall corrections.

The particle mass inventory was scaled by the particle density times the volume of the bed. Note that the resolution increases from left to right. One data point (for a grid length of 2.056 *du*) obtained from the filtered model simulations with wall corrections and no slip BC for both phases was also included. See caption of Figure 7 for the simulation conditions.

Figures 5a–c display the variation of the filtered drag coefficient, particle phase horizontal normal stress and shear viscosity with the distance from the wall, extracted from the kinetic theory model simulations for three different channel widths, given in the figure legend. (For each width, the results are shown for one-half of the channel width.) All the filtered quantities have been scaled with the corresponding quantities extracted from the core region (which were found to be nearly the same for all three channel widths). The results obtained with different channel widths nearly collapse (to within the confidence limit indicated by the error bars), clearly indicating that the wall effect should not be measured as a fraction of the channel width; instead it should be viewed in terms of actual distance (or made dimensionless using a length scale other than the channel width) from the wall.

In the figures presented above, we scaled the distance with v_t^2/g, which is the same scale we used to make filter length dimensionless. To ascertain that this scaling is appropriate, we performed simulations with two different particle diameters (75 and 100 μm). The lines in Figures 5a–c were generated using the 75 μm particles, while the squares were obtained for 100 μm particles. For both sets, the variation of the filtered closures with distance from the channel wall collapsed onto the same curves confirming that the scaling is indeed appropriate.

We then investigated the effect of flow conditions, such as particle mass flux and gas velocity, and the wall BCs (particle-wall restitution coefficient and specularity coefficient for the Johnson and Jackson BC) on the wall corrections to the filtered quantities. Among these, only wall-particle specularity coefficient had a measurably significant effect (in the 2D system studied here).

To study the sensitivity of the wall corrections to the specularity coefficient φ, we carried out simulations for five different values of φ: 0, 0.0001, 0.3, 0.6, and 1 in a channel with a width of 102.8 *du*. Snapshots of the particle phase volume fraction field extracted from two of these simulations (for $\varphi = 0.0001$ and 0.6) are shown in Figure 2. It has been reported that φ has a significant effect on the particle concentration near the wall; more specifically, a lower specularity coefficient yields higher particle concentration near the wall.[46,47,49] This is indeed what we see in these snapshots; particles tend to accumulate more and more as the specularity coefficient reaches free slip limit. It is also apparent that strands and clusters in the wall vicinity orient themselves in the vertical direction more for the lower specularity coefficient values. Figures 6a–c display the variation of scaled filtered drag coefficient, particle phase horizontal normal stress and shear viscosity with the distance from the wall for various φ values. It is clear that the value of φ has a quantitative effect on the wall corrections, but the dependence on φ nearly vanishes for $\varphi > 0.6$.

The correlations summarized in Table 2 capture the results on wall corrections to the filtered model closures and the specularity coefficient dependence described above.

Wall boundary conditions for the filtered equations

It is generally believed that in high-velocity flows of densely loaded gas-particle mixtures through large risers the vertical pressure gradient is largely due to the particle hold-up and the wall shear is only weakly relevant.[53] To test this, we calculated wall shear stress per unit height (under SSS conditions) from highly resolved kinetic theory-based two-fluid model simulations (with $\varphi = 0.6$) for two different channel widths, 61.68 and 102.8 *du* and found that wall shear supported $\sim$3% and $\sim$1% of the weight of the particles, respectively. When φ was lowered to 0.0001 in the 61.68 *du* wide channel, the wall shear stress supported only 0.003% of the weight of the particles. These comparisons confirm that the wall shear stress is considerably small compared to the weight of the particles in the channel and that the primary role of the wall is the "no penetration condition." With this in mind, we have set in the remainder of this study the wall BC for the filtered equations at the bounding walls in 2D systems as free slip for the particle phase. The observation from Figure 4c that the filtered shear viscosity *in the immediate vicinity of the walls* is considerably smaller than that for the bulk region (at a comparable particle volume fraction) provides further support for such simple BCs.

One can readily extrapolate the above analysis for the particle phase to the gas phase. We simply note here that the effective BC for the gas phase approaches free slip as the filter length increases, just as in the case of the particle phase. Thus, for modestly large filters (of the order of a few cms for the FCC particles mentioned in Table 1), one can use free slip BC for both phases as a good first approximation in 2D simulations. Here, it should be noted that if the tube diameter (or channel width) is small, the wall effect is expected to become more important and free slip BC may not be a good choice for wall boundaries. However, the filtered models will not be necessary for these computationally affordable simulations.

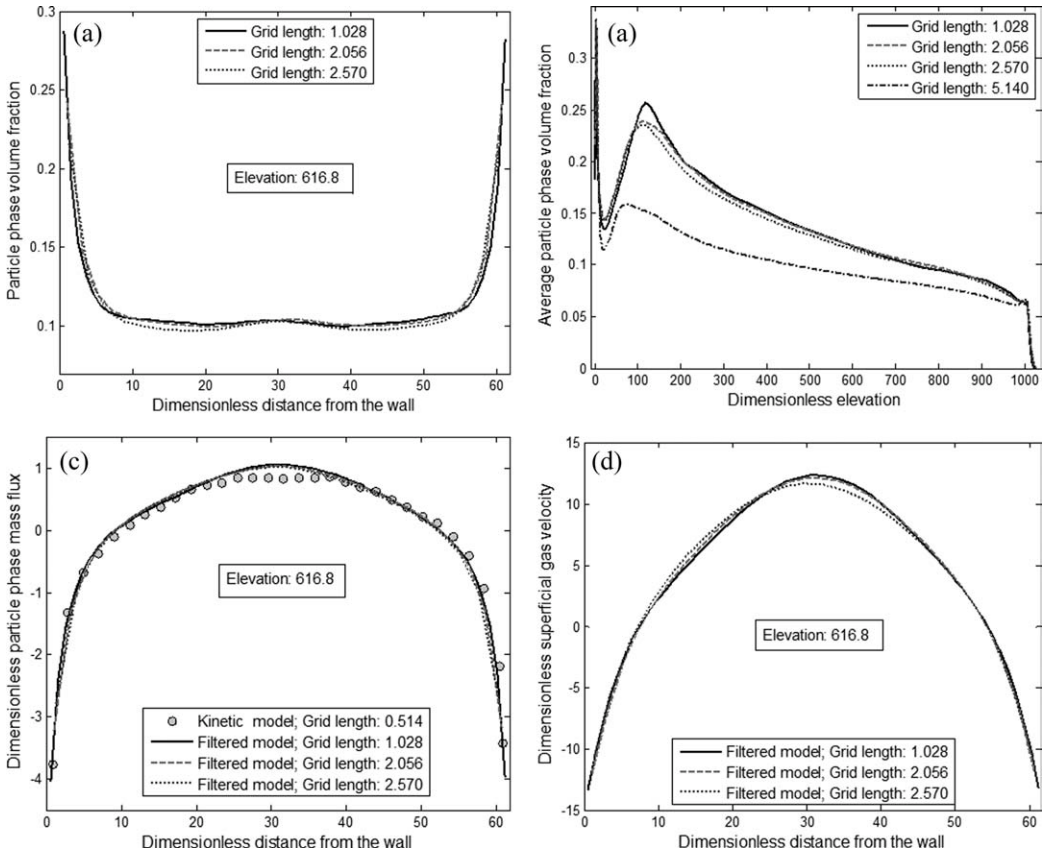

Figure 9. (a) The variation of temporally and laterally averaged particle phase volume fraction with the elevation in the 2D channel.

The variation of time-averaged (b) particle phase volume fraction, (c) axial particle phase mass flux, and (d) axial superficial gas velocity with the dimensionless distance from the wall at an elevation of 616.6 *du*. Results were obtained from simulations of a filtered model with a filter length of 4.112 *du* (including wall corrections) and different grid lengths, shown in the figure legends. See caption of Figure 7 for the simulation conditions. The circles in Figure 9(b) were obtained by solving the kinetic theory-based model using a grid length of 0.514 *du*.

Grid resolution dependence of channel flow simulations

Figures 7a–c show snapshots in the SSS for kinetic theory simulations (of gas-particle flows in a 2D channel as in Figure 1) at three different grid resolutions, while Figures 7d–f show simulations with a filtered model corresponding to a filter length of 4.112 *du* (and including wall corrections). It is readily apparent that finer and finer structures got resolved with increasing grid resolution for the kinetic theory cases, while this was not the case with filtered model simulations.

Figure 8 shows the variation of the time-averaged (scaled) particle phase mass inventory with grid resolution, determined from the simulations with the kinetic theory and the filtered model with and without wall corrections. (Although we had established that wall corrections to the closures in filtered model are appreciable, we performed filtered model simulations with and without wall corrections to learn more about the extent of influence brought about by the wall corrections.) The particle mass inventory was scaled with the product of the particle density and the volume of the bed. The grid resolution increases from left to right. It is readily seen that the particle mass inventory predicted by the kinetic theory model, indicated with light gray squares, became only grid resolution independent when the grid length was smaller than 1.028 *du*. However, an inspection of the lateral particle volume fraction and mass flux profiles (not shown) revealed that this grid length was not sufficient to obtain grid resolution independent results and that the kinetic theory model did not show any concrete evidence of converging even at the highest resolution affordable.

In the case of filtered model simulations with wall corrections, represented by black diamond-shaped symbols in Figure 8, as the grid resolution was increased, the particle phase mass inventory increased initially, but essentially became grid resolution independent once the grid length became smaller or equal to $\sim$2.056 *du*, which is one-half of the filter length.

Figure 9a compares the variation of temporally and laterally averaged particle volume fraction (in the SSS) with the elevation in the 2D channel obtained from simulations of the filtered model (including wall corrections) for four grid resolutions. At the bottom of the riser and near the top of the channel, the particle volume fraction changes rapidly with elevation, indicating strong entrance and exit effect. At the very bottom of the channel, the particles get accelerated by the incoming gas; therefore the average volume fraction initially decreases. At higher elevations, the particles near the wall have downward velocities and these descending particles encounter the ascending particles at the bottom and

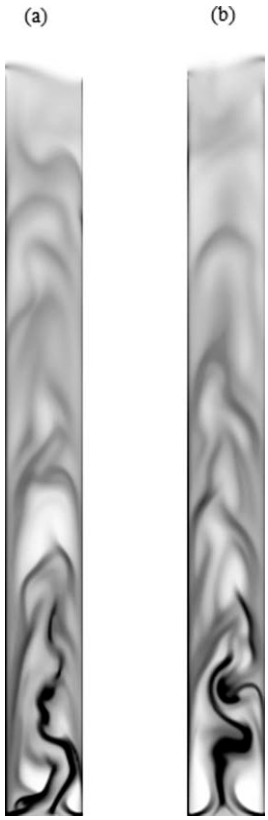

Figure 10. Snapshots of the particle phase volume fraction field extracted from the 2D simulation of the filtered model equations extracted with a filter length of (a) 4.112 *du* and (b) 8.224 *du*.

Simulation conditions: The dimensionless inlet gas and particle phase superficial velocities are 4.259 and 0.109, respectively. The physical conditions corresponding to this simulation are listed in Table 1. The inlet particle phase volume fraction is 0.07. Grid length: 2.056 *du*. Free slip BC was used for both phases at all walls. Wall corrections (extracted from kinetic theory simulations with $\varphi = 0.6$) are included. Channel width and height are 102.8 and 1028 *du*, respectively. The gray scale axis ranges from $\phi_s = 0.00$ (white) to $\phi_s = 0.45$ (black).

this leads to a rapid increase in volume fraction at an elevation of about 100–150 *du*; in other words, the ascending particles at the bottom capture the descending particles and redirect them to flow upwards. In the middle region, the variation of particle volume fraction with elevation is gradual; the average particle phase volume fraction decreases with increasing elevation. The variation pattern is similar for all grid resolutions at all elevations. It is clear from the figure that the two uppermost curves, representing the average particle volume fraction profile determined with grid lengths of 1.028 and 2.056 *du*, essentially overlap. Figures 9b–d show the corresponding variations of the time-averaged particle phase volume fraction, particle mass flux and gas velocity (respectively) with dimensionless distance from the bounding wall at an elevation of 616.8 *du* for three different dimensionless grid lengths. At all three resolutions, particles accumulate in the vicinity of the walls, and a dilute core region is observed. It is clear from these figures that lateral profiles are nearly identical for grid lengths of 1.028 and 2.056 *du*. Similar results were obtained at other elevations away from the entrance and exit effects. Figure 9c includes the time-averaged particle mass flux results obtained from the most highly resolved kinetic theory model simulations done in this study. The agreement between the filtered and kinetic theory models is good, clearly indicating the filtered model solutions do indeed correspond to the kinetic theory model from which they were developed. This is required of a successful filtered model and it serves as a verification of the filtered model approach. Additional such verifications are provided later in this manuscript.

In the above examples, we employed free slip BCs for the gas and particle phases at all bounding walls. If one replaces the free slip conditions with no slip for both phases, the mass holdup predicted by the filtered model decreased by ~30% (see Figure 8). These two extremes (free slip and no slip) serve as bounds and thus give an idea about the extent of the changes in the mean flow characteristics that can come about altering the BCs. In this example, the free slip BCs led to better match with the kinetic theory results, for reasons discussed earlier.

Figure 8 also shows the results obtained when the wall corrections were turned off in the filtered model (while using free slip BCs). Nearly grid resolution independent solution was still achieved as when the wall corrections were included; however, a much smaller mass inventory was predicted without wall corrections leading to quantitatively very different results from that obtained with the highly resolved kinetic theory model simulation. This illustrates that wall corrections are important for quantitative accuracy. (We also explored the effect of including the wall corrections to the filtered drag coefficient, particle phase horizontal normal stress and shear viscosity one at a time or two at a time on the predictions of the filtered model equations. This analysis revealed that the corrections affected the results predicted by the filtered model simulations quantitatively—namely, increase or decrease particle phase mass inventory in the channel, but did not affect the grid resolution independence of these results. Quantitative comparison with the kinetic theory results were obtained only when all three corrections were included.)

Grid resolution requirement for filtered models. As the closures for the filtered model were derived by averaging over structures smaller than a chosen filter length, Δ_f, it is reasonable to demand that solution of the filtered model should not yield fine structures much smaller than the filter length; if it did, it suggests weakness in the model formulation. Thus, for a satisfactorily constructed filtered model, the grid length, Δ_g, required for grid-independent solutions should scale with the filter length. The results presented in Figures 8 and 9 suggest that $\Delta_g \sim 0.5\ \Delta_f$ is essentially adequate. With this in mind, we propose that the grid length be set as $\Delta_g \sim 0.3 - 0.5\Delta_f$ in filtered model simulations.

Addition of a particle phase bulk viscosity term to the filtered model. In the filtered model, the particle phase stress was modeled as follows:

$$\sum\nolimits_s = \overline{p_{s,\text{filtered}}}\mathbf{I} - \overline{\mu_{b,\text{filtered}}}(\nabla\cdot\bar{\mathbf{v}})\mathrm{I} - \overline{\mu_{s,\text{filtered}}}\left(\nabla\bar{\mathbf{v}} + (\nabla\bar{\mathbf{v}})^T - \tfrac{2}{3}(\nabla\cdot\bar{\mathbf{v}})\mathrm{I}\right) \quad (3)$$

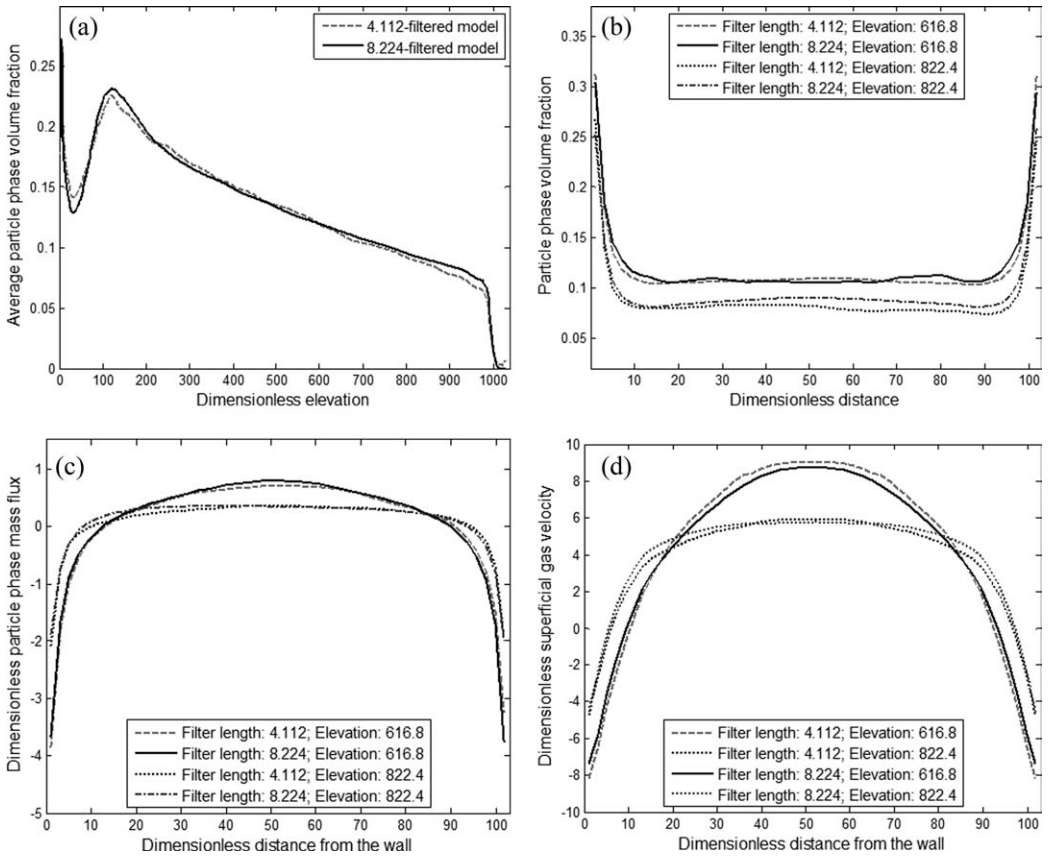

Figure 11. (a) The variation of temporally and laterally averaged particle volume fraction with the elevation in the 2D channel, determined from simulations of filtered models with filter lengths of 4.112 and 8.224 *du*.

The variation of time-averaged (b) particle phase volume fraction, (c) axial particle phase mass flux, and (d) axial superficial gas velocity with the dimensionless distance from the wall at two elevations (616.8 and 822.4 *du*). Grid length: 2.056 *du*. See caption of Figure 10 for the simulation conditions.

where $\overline{\mu_{s,\text{filtered}}}$ and $\overline{\mu_{b,\text{filtered}}}$ are the shear and bulk viscosities, respectively. As we did not determine $\overline{\mu_{b,\text{filtered}}}$ by filtering the results from highly resolved kinetic theory model simulations, we had set it to zero in the examples presented above. We repeated the simulations in Figure 9 while setting the filtered bulk viscosity to be the same as the filtered shear viscosity, and found virtually no change. It is therefore reasonable to conclude that a bulk viscosity term in the filtered model is not important for channel flows. We also studied the effect of adding *a mesoscale viscosity term to the gas phase* filtered model equations and found it to have a very weak effect (if any) on the channel flow results predicted by the filtered model simulations.

The effect of filter length on predictions of the filtered models

Snapshots of particle volume fraction fields in the SSS for gas-particle flow in vertical 2D channel (whose width is 102.8 *du*) obtained by solving filtered models with filter lengths of 4.112 and 8.224 *du* are shown in Figures 10a, b, respectively. The simulation with coarser filter yielded slightly coarser structures, as expected.

The variation of temporally and laterally averaged particle volume fraction with elevation in the channel, obtained in the SSS of these two simulations is presented in Figure 11a. It is apparent that both filtered models yielded nearly identical results. The average particle phase mass inventory scaled with the product of the channel volume and particle density was computed to be 0.135 and 0.136 for the filtered models with filter lengths of 4.112 and 8.224 *du*, respectively.

Figures 11b–d present the variation of the time-averaged particle phase volume fraction, axial particle phase mass flux, and axial superficial gas velocity with the distance from the wall at two elevations, obtained from the two filtered models; once again the agreement is good. In all the results presented in Figures 10 and 11, we have used the same grid length of 2.056 *du*, which is one half the size of the smaller filter used in the comparison. We simply note that when the filtered model with the larger filter was repeated using a grid length of 4.112 *du*, virtually the same results were obtained; so the grid length recommendation made earlier still applies.

These observations that filtered models corresponding to two different filter lengths (4.112 and 8.224 *du*) yielded comparable results provide support for the soundness of the approach.

Further verification of the filtered model

Earlier in this manuscript, we provided one comparison between the results obtained with a filtered two-fluid model and (highly resolved simulations of) the kinetic theory-based

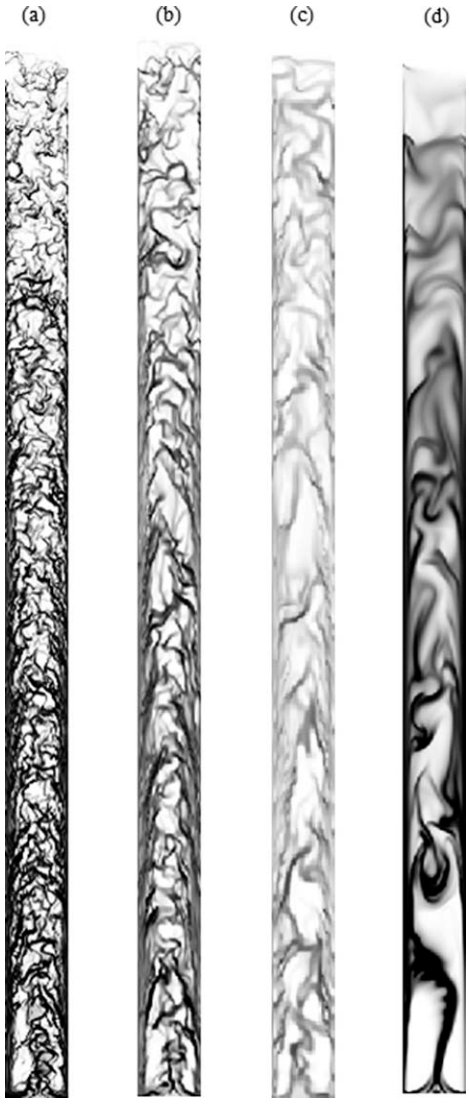

Figure 12. Snapshot of the particle phase volume fraction field extracted from the 2D simulation of (a) the kinetic theory model equations with 0.514 *du* grids, (b) the kinetic theory model equations with 1.028 *du* grids, (c) the kinetic theory model equations with 2.056 *du* grids, (d) the filtered model equation with 1.028 *du* grids.

Wall corrections (extracted from kinetic theory simulations with $\varphi = 0.0001$) were included in the closures for the filtered model equations. Simulation conditions: The dimensionless inlet gas and particle phase superficial velocities are 4.259 and 0.109, respectively. The physical conditions corresponding to this simulation are listed in Table 1. The inlet particle phase volume fraction is 0.07. Free slip BC was imposed for both phases at all walls for simulations of the filtered models, whereas in the kinetic theory-based simulations, partial slip BC for the particle phase ($\varphi = 0.0001$) and free slip BC for the gas phase were used. Channel width and height are 61.68 and 1028 *du*, respectively. The gray scale axis ranges from $\phi_s = 0.00$ (white) to $\phi_s = 0.45$ (black).

two-fluid model, for the case of a very bumpy wall (with $\varphi = 0.6$). We now consider the case of a much smoother wall with $\varphi = 0.0001$. Snapshots of the particle volume fraction field (in the SSS) from the kinetic model simulations with grid lengths of 0.514, 1.028, and 4.112 *du* and the filtered model simulation (with filter and grid lengths of 4.112 and 1.028 *du*, respectively) are shown in Figures 12a–d. As shown earlier in Figure 7, the kinetic theory model simulations yielded finer and finer structures as the grid length decreased.

Figure 13 compares the variation of temporally and laterally averaged particle volume fraction with the elevation in the 2D channel obtained from simulations of the kinetic theory model for four grid resolutions and that from the filtered model simulations with a grid length of 1.028 *du*. The grid resolution dependence of the kinetic theory model is clearly seen in the figure. The filtered model profile is slightly above the kinetic model simulation with 0.514 (*du*) grids and appears to provide an asymptotic value for the results that would be predicted by the kinetic theory model (at an even finer resolution).

The variation of the time-averaged particle phase volume fraction, dimensionless axial particle phase mass flux and superficial gas velocity (predicted by both models) with the dimensionless distance from one of the vertical bounding walls are presented in Figures 14–16, respectively, with panels a and b in each figure corresponding to two different elevations. These figures clearly show the grid resolution dependence of the results predicted by the kinetic theory model. It is also apparent in the figures that the results predicted by the filtered model and the kinetic model (with 0.514 *du* grids) are comparable. (The results obtained with the filtered model for a grid length of 2.056 *du* are very close to that reported in these figures and hence are not shown.) These figures lend further credence to the filtered model approach to obtaining solutions for such flow problems.

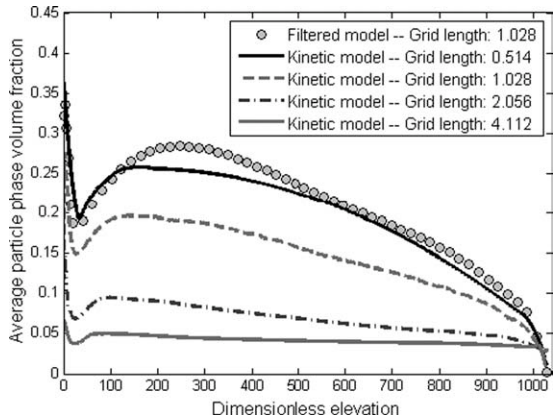

Figure 13. The variation of temporally and radially averaged particle volume fraction with the elevation in the 2D channel, whose snapshots are shown in Figure 12.

Results were obtained from simulations of a filtered model with a filter length of 4.112 *du* (including wall corrections) and different grid sizes. Results shown as lines were obtained from simulations of kinetic theory-based model with different grid lengths, shown in the figure legend. The circles were obtained by solving the filtered model (filter length: 4.112 *du*) using a grid length of 1.028 *du*. See caption of Figure 12 for the simulation conditions.

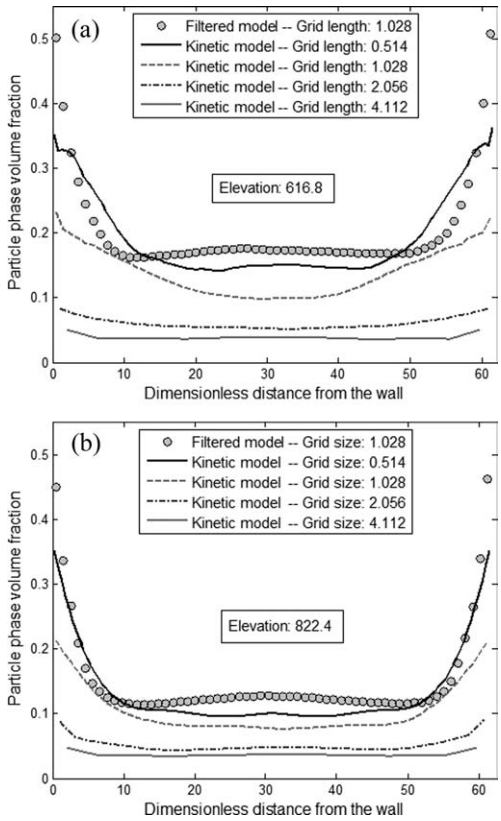

Figure 14. The variation of dimensionless time-averaged particle phase volume fraction with the dimensionless distance from the west (left) wall at two elevations (a) 616.8 *du*; (b) 822.4 *du*.

Results shown as lines were obtained from simulations of kinetic theory-based model with different grid lengths, shown in the figure legends. See caption of Figure 12 for the simulation conditions. The circles were obtained by solving the filtered model (filter length: 4.112 *du*) using a grid length of 1.028 *du*.

CPU time comparison

Figure 17 shows the CPU times required to compute one second of flow for the kinetic theory-based two-fluid (gray squares) and the filtered model with a filter length of 4.112 *du* (black circles) at various grid resolutions. All the simulation conditions are described in the figure caption (and in Figure 7). The simulations reported in this were performed on Dual quad core Intel Xeon E5420 processors running at 2.50 GHz. The filtered-model-based simulation with a grid length of 1.028 *du* ran ~four times faster than the kinetic theory-based simulation at the same resolution. This can be attributed to the finer structures contained in the kinetic theory model, see Figure 7. Note that one does not need to use such a small 1.028 *du* grid length with the filtered model; when the grid length in the filtered model simulation is increased to 2.056 *du*, it ran ~30 and 300 times faster than the kinetic theory-based two-fluid model with grid lengths of 1.028 and 0.514 *du*, respectively. When the specularity coefficient was changed to 0.0001, the filtered-model simulation with filter and grid lengths of 4.112 and 1.028 *du* (respectively) ran ~5 and 40 times faster than the kinetic theory-based simulation with grid lengths of 1.028 and 0.514 *du*, respectively. (Once again, a grid length of 2.056 *du* would have sufficed for this filtered model, which would have lowered the computational time for the filtered model by a factor of ~7.5.).

Next, we compared the simulation times (for flow in the 102.8 *du*-wide channel) for filtered models with two different filter lengths and a grid length of 2.056 *du*. The model with a filter length of 8.224 *du* ran three times faster than that with a filter length of 4.112 *du*. This can be attributed to the finer structures contained in the latter model. Note that one does not need to use a grid length of 2.056 *du* for a model with a filter length of 8.224 *du*; the filtered model with a filter length of 8.224 *du* and grid lengths of 2.570 and 4.112 ran ~7 and 25 times faster than the filtered model with a filter length of 4.112 *du* and a grid length of 2.056 *du*. Combining this example with the one in the previous paragraph, we project that a filtered model with a filter length of 8.224 *du* (and 4.112 *du* grids) will yield solution ~7500 times faster than the kinetic theory model with a grid length of 0.514 *du* (which was seen to be necessary to get nearly grid independent solution).

For the 75 μm particles in Table 1, a filter length of 8.224 *du* translates to a filter length of 4 cm. In large-scale processes, one typically uses even larger grids and so one would

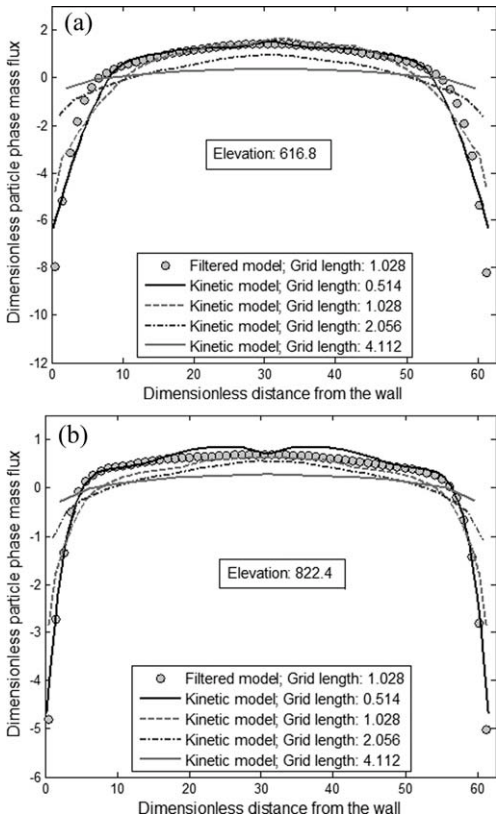

Figure 15. The variation of dimensionless time-averaged particle phase mass flux with the dimensionless distance from the west (left) wall at two elevations (a) 616.8 *du*; (b) 822.4 *du*.

Results shown as lines were obtained from simulations of kinetic theory-based model with different grid lengths, shown in the figure legends. See caption of Figure 12 for the simulation conditions. The circles were obtained by solving the filtered model (filter length: 4.112 *du*) using a grid length of 1.028 *du*.

use even larger filters and correspondingly faster simulations (when compared with highly resolved kinetic theory model simulations whose required grid resolution is not likely to change with process vessel size). Finally, when one considers 3D simulations, the difference between filtered and well-resolved kinetic theory models is expected to be even larger.

In summary, filtered models allow us to study the large structures in gas-particle flows without having to resolve smaller structures and in a computationally affordable and faster manner.

Summary

We have investigated the effect of the bounding walls on the closure relationships for the filtered two-fluid model equations through a set of 2D flow simulations in a channel equipped with bounding walls and inlet and outlet regions. This study, which is valid for the particle volume fraction range typical of gas-particle flows in risers, reveals that:

(a) Closures for the filtered drag coefficient and particle phase stress depend not only on particle volume fraction and the filter length but also on the distance from the wall.

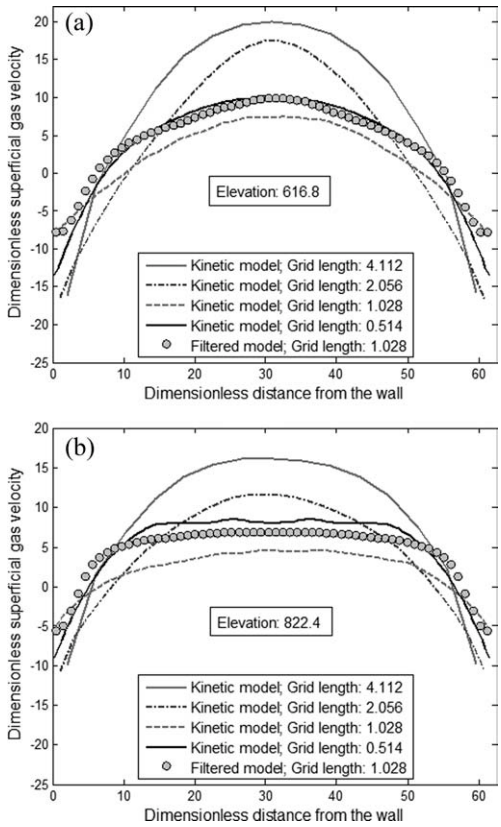

Figure 16. The variation of dimensionless time-averaged axial superficial gas velocity with the dimensionless distance from the west (left) wall at two elevations (a) 616.8 *du*; (b) 822.4 *du*.

Results shown as lines were obtained from simulations of kinetic theory-based model with different grid lengths, shown in the figure legends. See caption of Figure 12 for the simulation conditions. The circles were obtained by solving the filtered model (filter length: 4.112 *du*) using a grid length of 1.028 *du*.

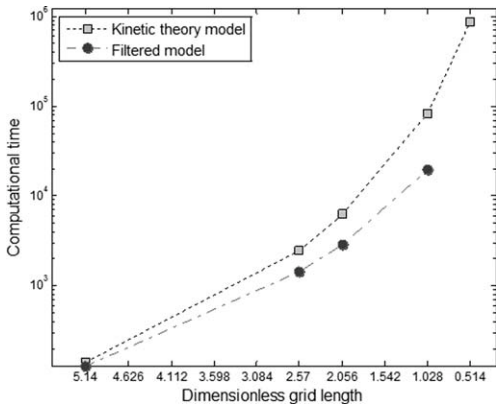

Figure 17. CPU times required to run one simulation second for the kinetic theory-based two-fluid model and a filtered model with a filter length of 4.112 *du* at different grid resolutions.

Note that the resolution increases from left to right. See caption of Figure 7 for the simulation conditions. The simulations were performed on Dual quad core Intel Xeon E5420 processors running at 2.50 GHz.

(b) The wall effect should not be measured as a fraction of the channel width; instead, it should be viewed in terms of the actual distance from the wall. The characteristic length to scale the distance from the wall is the same as that used to scale the filter length.

(c) The wall corrections to the filtered closures are nearly independent of the mean particle volume fraction in the filtering region.

(d) The wall corrections to the filtered closures are nearly independent of the filter lengths considered in this study.

(e) The simplest effective BC for the filtered equations at the bounding walls is free slip BC.

Filtered model simulations performed in this study revealed the following:

(a) Grid resolution independent solutions resulted when the grid length is ~half the filter length or smaller.

(b) Filtered models did indeed yield the same coarse statistical results as highly resolved simulations of kinetic theory-based two-fluid model (which was used to derive the filtered models).

(c) Filtered models with two different filter lengths were shown to afford the same coarse statistical results.

(d) Filtered model simulations required significantly less computational time when compared with highly resolved kinetic theory-based two-fluid model simulations.

This study establishes the fidelity of the filtered model, but two important tasks remain: (a) It would be useful to establish general closures for the filtered model in terms of particle volume fraction and filter length so that they can be broadly used by researchers; (b) The filtered model predictions should be compared against experimental data. These will be described in future publications.

Acknowledgments

This work was supported by the US Department of Energy (grants: CDE-FC26-00NT40971 and DE-PS26-05NT42472-11) and the Exxon-Mobil Research & Engineering Company. Igci acknowledges summer training on MFIX at the National Energy Technology Laboratory,

Morgantown, WV. We thank Sreekanth Pannala, Madhava Syamlal, Chris Guenther, Ronald Breault, and Sofiane Benyahia for their assistance throughout the course of this study.

Notation

d_p = particle diameter (m)
e_p = coefficient of restitution for particle-particle collisions
e_w = coefficient of restitution for wall-particle collisions
Fr_f = Froude number based on filter length = $v_t^2/g\Delta_f$
Fr_g = Froude number based on grid length = $v_t^2/g\Delta_g$
g, $\mathbf{g}$ = acceleration due to gravity (m/s^2)
g_o = value of radial distribution function at contact
$\overline{p_{s,filtered}}$ = filtered particle phase pressure (kg/m s^2)
$\overline{p_{s,filtered,d}}$ = $\overline{p_{s,filtered,d}}$ made dimensionless; $\overline{p_{s,filtered,d}} = \overline{p_{s,filtered}}/\rho_s v_t^2$
$\overline{p_{s,filtered,xx}}$ = filtered particle phase horizontal normal stress (kg/m s^2)
$\overline{p_{s,filtered,xx,core}}$ = $\overline{p_{s,filtered,xx}}$ extracted from the core region of the 2D channel (kg/m s^2)
$\overline{p_{s,filtered,xx,periodic}}$ = $\overline{p_{s,filtered,xx}}$ extracted from periodic BC simulations (kg/m s^2)
$\overline{p_{s,filtered,xx,d}}$ = $\overline{p_{s,filtered,xx,d}}$ made dimensionless; $\overline{p_{s,filtered,xx,d}} = \overline{p_{s,filtered,xx}}/\rho_s v_t^2$
$\overline{p_{s,filtered,xx,scaled}}$ = $\overline{p_{s,filtered,xx}}$ scaled with $\overline{p_{s,filtered,xx,core}}$; $\overline{p_{s,filtered,xx,scaled}} = \overline{p_{s,filtered,xx}}/\overline{p_{s,filtered,xx,core}}$
$\overline{p_{s,kinetic}}$ = filtered value of particle phase pressures in the kinetic theory model (kg/m.s^2)
$\mathbf{q}$ = flux of granular energy (kg/s^3)
v_t = terminal settling velocity (m/s)
$\mathbf{v}$ = particle phase velocity in the microscopic two-fluid model (m/s)
$\overline{\mathbf{v}}$ = filtered particle phase velocity (m/s)
$\mathbf{v}'$ = fluctuations in particle phase velocity (m/s)
$\mathbf{x}$, $\mathbf{y}$ = position vectors (m)
x_d = dimensionless distance from the west (left) wall

Greek letters

$\overline{\beta_{filtered}}$ = filtered drag coefficient (kg/m^3 s)
$\overline{\beta_{filtered,core}}$ = $\overline{\beta_{filtered}}$ extracted from the core region of the 2D channel (kg/m^3 s)
$\overline{\beta_{filtered,periodic}}$ = $\overline{\beta_{filtered}}$ extracted from periodic BC simulations (kg/m^3 s)
$\overline{\beta_{filtered,d}}$ = dimensionless filtered drag coefficient = $\overline{\beta_{filtered}} v_t/\rho_s g$
$\overline{\beta_{filtered,scaled}}$ = $\overline{\beta_{filtered}}$ scaled with $\overline{\beta_{filtered,core}}$; $\overline{\beta_{filtered,scaled}} = \overline{\beta_{filtered}}/\overline{\beta_{filtered,core}}$
ϕ_s, ϕ_g = particle and gas phase volume fractions, respectively
$\phi_{s,max}$ = maximum particle volume fraction
$\overline{\phi_s}$, $\overline{\phi_g}$ = filtered particle and gas phase volume fractions, respectively
ρ_s, ρ_g = particle and gas densities, respectively (kg/m^3)
Δ_f = filter length (m)
Δ_g = grid length (m)
$\overline{\overline{\sigma_s}}$ = particle phase stress tensor in the kinetic theory model (kg/m s^2)
$\mathbf{\Sigma}_s$ = filtered total particle phase stress (kg/m s^2)
λ_s = granular thermal conductivity (kg/m s)
μ_g = gas phase viscosity (kg/m s)
μ_s = shear viscosity of the particle phase appearing in the kinetic theory model (kg/m s)
$\overline{\mu_{b,filtered}}$, $\overline{\mu_{s,filtered}}$ = bulk and shear viscosities of the particle phase appearing in the filtered two-fluid model (kg/m s)
$\overline{\mu_{s,filtered,d}}$ = $\overline{\mu_{s,filtered}}$ made dimensionless; $\overline{\mu_{s,filtered,d}} = \overline{\mu_{s,filtered}} g/\rho_s v_t^3$
$\overline{\mu_{s,filtered,core}}$ = $\overline{\mu_{s,filtered}}$ extracted from the core region of the 2D channel (kg/m s)
$\overline{\mu_{s,filtered,periodic}}$ = $\overline{\mu_{s,filtered}}$ extracted from periodic BC simulations (kg/m s)
$\overline{\mu_{s,filtered,scaled}}$ = $\overline{\mu_{s,filtered}}$ scaled with $\overline{\mu_{s,filtered,core}}$; $\overline{\mu_{s,filtered,scaled}} = \overline{\mu_{s,filtered}}/\overline{\mu_{s,filtered,core}}$
θ_s = granular temperature (m^2/s^2)
φ = wall specularity coefficient

Literature Cited

1. Schnitzlein MG, Weinstein H. Flow characterization in high-velocity fluidized beds using pressure fluctuations. *Chem Eng Sci*. 1988;43:2605–2614.
2. Gidaspow D. *Multiphase Flow and Fluidization*. San Diego, CA: Academic Press, 1994.
3. Nieuwland JJ, Annaland MV, Kuipers JAM, van Swaaij WPM. Hydrodynamic modeling of gas/particle flows in riser reactors. *AIChE J*. 1996;42:1569–1582.
4. Neri A, Gidaspow D. Riser hydrodynamics: simulation using kinetic theory. *AIChE J*. 2000;46:52–67.
5. Weinstein H, Shao M, Schnitzlein M. *Radial variation in solid density in high velocity fluidization*. In: Basu P, editor. *Circulating Fluidized Bed Technology*. Elmsford, NY: Pergamon, 1986:201.
6. Bader R, Findlay J, Knowlton T. *Gas/solid flow patterns in a 30.5-cm diameter circulating fluidized bed*. In: Basu P, Large JF, editors. *Circulating Fluidized Bed Technology*. Vol II. Elmsford, NY: Pergamon, 1988:123–ndash.
7. Chen JC. Clusters. *AIChE Sym S*. 1996;92:1–5.
8. Sharma AK, Tuzla K, Matsen J, Chen JC. Parametric effects of particle size and gas velocity on cluster characteristics in fast fluidized beds. *Powder Technol*. 2000;111:114–122.
9. Harris AT, Davidson JF, Thorpe RB. The prediction of particle cluster properties in the near wall region of a vertical riser (200157). *Powder Technol*. 2002;127:128–143.
10. Jackson R. *The Dynamics of Fluidized Particles*. Cambridge, UK: Cambridge University Press, 2000.
11. Syamlal M, Rogers W, O'Brien TJ. *MFIX Documentation*. Morgantown, WV: U.S. Department of Energy, Federal Energy Technology Center, 1993.
12. Agrawal K, Loezos PN, Syamlal M, Sundaresan S. The role of meso-scale structures in rapid gas-solid flows. *J Fluid Mech*. 2001;445:151–185.
13. Wang J. High-resolution Eulerian simulation of RMS of solid volume fraction fluctuation and particle clustering characteristics in a CFB riser. *Chem Eng Sci*. 2008;63:3341–3347.
14. Wang J, van der Hoef MA, Kuipers JAM. Why the two-fluid model fails to predict the bed expansion characteristics of Geldart A particles in gas-fluidized beds: a tentative answer. *Chem Eng Sci*. 2009;64:622–625.
15. Sundaresan S. Modeling the hydrodynamics of multiphase flow reactors: current status and challenges. *AIChE J*. 2000;46:1102–1105.
16. Qi H, Li F, You C. Modeling of drag with the Eulerian approach and EMMS theory for heterogeneous gas-solid two-phase flow. *Chem Eng Sci*. 2007;62:1670–1681.
17. O'Brien TJ, Syamlal M. *Particle cluster effects in the numerical simulation of a circulating fluidized bed*. In: Avidan A, editor. *Circulating Fluidized Bed Technology. IV. Proceedings of the Fourth International Conference on Circulating Fluidized Beds*, Hidden Valley Conference Center, Somerset, PA, August 1–5, 1993.
18. Boemer A, Qi H, Hannes J, Renz U. Modelling of solids circulation in a fluidized bed with Eulerian approach. 29th IEA-FBC Meeting, Paris, France, Nov. 24–26, 1994.
19. Heynderickx GJ, Das AK, De Wilde J, Marin GB. Effect of clustering on gas-solid drag in dilute two-phase flow. *Ind Eng Chem Res*. 2004;43:4635–4646.
20. McKeen T, Pugsley T. Simulation and experimental validation of a freely bubbling bed of FCC catalyst. *Powder Technol*. 2003; 129:139–152.
21. Yang N, Wang W, Ge W, Wang L, Li J. Simulation of heterogeneous structure in a circulating fluidized-bed riser by combining the two-fluid with the EMMS approach. *Ind Eng Chem Res*. 2004;43:5548–5561.
22. Yang N, Wang W, Ge W, Li J. CFD simulation of concurrent-up gas-solid flow in circulating fluidized beds with structure dependent drag coefficient. *Chem Eng J*. 2003;96:71–80.
23. Li J, Kwauk M. Exploring complex systems in chemical engineering—the multi-scale methodology. *Chem Eng Sci*. 2003;58:521–535.
24. Wang J, van der Hoef MA, Kuipers JAM. Coarse grid simulation of bed expansion characteristics of industrial-scale gas-solid bubbling fluidized beds. *Chem Eng Sci*. 2010;65:2125–2131.
25. Krishna R, van Baten JM. Using CFD for scaling up gas-solid bubbling fluidized bed reactors with Geldart A powders. *Chem Eng J*. 2001;82:247–257.
26. Dasgupta S, Jackson R, Sundaresan S. Turbulent gas-particle flow in vertical risers. *AIChE J*. 1994;40:215–228.

27. Hrenya CM, Sinclair JL. Effects of particle-phase turbulence in gas-solid flows. *AIChE J*. 1997;43:853–869.
28. Andrews AT IV, Loezos PN, Sundaresan S. Coarse-grid simulation of gas-particle flows in vertical risers. *Ind Eng Chem Res*. 2005;44:6022–6037.
29. Igci Y, Andrews IV AT, Sundaresan S, Pannala S, O'Brien T. Filtered two-fluid models for fluidized gas-particle suspensions. *AIChE J*. 2008;54:1431–1448.
30. Zhang DZ, VanderHeyden WB. The effects of mesoscale structures on the macroscopic momentum equations for two-phase flows. *Int J Multiphase Flow*. 2002;28:805–822.
31. Li J. Multi-scale modeling and method of energy minimization in two-phase flow. Ph.D. thesis. Institute of Chemical Metallurgy, Chinese Academy of Sciences, Beijing, 1987.
32. Li J, Tung Y, Kwauk M. *Energy transport and regime transition of particle-fluid two-phase flow*. In: Basu P, Large JF, editors. *Circulating Fluidized Bed Technology II*. Oxford: Pergamon Press, 1988:75.
33. Li J, Cheng C, Zhang Z, Yuan J. The EMMS model, its application, development and updated concepts. *Chem Eng Sci*. 1999;54:5409–5425.
34. Li J, Zhang Z, Ge W, Sun Q, Yuan J. A simple variation criterion for turbulent flow in pipe. *Chem Eng Sci*. 1999;54:1151–1154.
35. Li J, Kwauk M. *Particle-Fluid Two-Phase Flow Energy-Minimization Multi-Scale Method*. Beijing: Metallurgical Industry Press, 1994.
36. Wang J, Ge W. Multi-scale analysis on particle-phase stresses of coarse particles in bubbling fluidized beds. *Chem Eng Sci*. 2006;61:2736–2741.
37. Lu B, Wang W, Li J, et al. Multi-scale CFD simulation of gas–solid flow in MIP reactors with a structure-dependent drag model. *Chem Eng Sci*. 2007;62:5487–5494.
38. Wang W, Li J. Simulation of gas–solid two-phase flow by a multi-scale CFD approach—Extension of the EMMS model to the sub-grid level. *Chem Eng Sci*. 2007;62:208–231.
39. Chalermsinsuwan B, Piumsomboon P, Gidaspow D. Kinetic theory based computation of PSRI riser: part I—estimate of mass transfer coefficient. *Chem Eng Sci*. 2009;64:1195–1211.
40. Lu B, Wang W, Li J. Searching for a mesh-independent sub-grid model for CFD simulation of gas-solid riser flows. *Chem Eng Sci*. 2009;64:3437–3447.
41. Wang W, Lu B, Li J. Choking and flow regime transitions: simulation by a multi-scale CFD approach. *Chem Eng Sci*. 2007;62:814–819.
42. Benyahia S. On the effect of subgrid drag closures. *Ind Eng Chem Res*. 2010;49:5122–5131.
43. Zou B, Li H, Xia Y, Ma X. Cluster structure in a circulating fluidized bed. *Powder Technol*. 1994;78:173–178.
44. Miller A, Gidaspow D. Dense, vertical gas-solid flow in a pipe. *AIChE J*. 1992;38:1801–1815.
45. Johnson P, Jackson R. Frictional-collisonal constitutive relations for granular materials, with application to plane shearing. *J Fluid Mech*. 1987;176:67–93.
46. Behyahia S, Syamlal M, O'Brien T. Evaluation of boundary conditions used to model dilute, turbulent gas/solids flows in a pipe. *Powder Technol*. 2005;156:62–72.
47. Almuttar A, Taghipour F. Computational fluid dynamics of a circulating fluidized bed under various fluidization conditions. *Chem Eng Sci*. 2008;63:1696–1709.
48. Benyahia S, Syamlal M, O'Brien TJ. Study of the ability of multiphase continuum models to predict core-annulus flow. *AIChE J*. 2007;53:2549–2568.
49. He J, Simonin O. Non-equilibrium prediction of particle-phase stress tensor in vertical pneumatic conveying gas-solids flows. *ASME FED*. 1993;166:253–263.
50. Jiradilok V, Gidaspow D, Damronglerd S, Koves WJ, Mostofi R. Kinetic theory based CFD simulation of turbulent fluidization of FCC particles in a riser. *Chem Eng Sci*. 2006;61:5544–5559.
51. Wang X, Jin B, Zhong W, Xiao R. Modeling on the hydrodynamics of a high-flux circulating fluidized bed with geldart group A particles by kinetic theory of granular flow. *Energy Fuel*. 2010;24:1242–1259.
52. Piomelli U, Balaras E. Wall-layer models for large-eddy simulations. *Annu Rev Fluid Mech*. 2002;34:349–374.
53. Chang H, Louge M. Fluid dynamic similarity of circulating fluidized-beds. *Powder Technol*. 1992;17:1293–1313.

Manuscript received June 28, 2010, and revision received Oct. 25, 2010.